Where is the real transform boundary in California?

John P. Platt and Thorsten W. Becker

Department of Earth Sciences, University of Southern California, Los Angeles, California 90089, USA (jplatt@usc.edu)

[1] The zone of highest geodetically defined strain rate in California does not everywhere coincide with the surface trace of the San Andreas Fault (SAF). To determine whether this reflects the pattern of long-term, permanent deformation, we analyzed the velocity field on swaths across the transform, located so as to avoid intersections among the major fault strands. Slip rates and flexural parameters for each fault were determined by finding the best fit to the velocity profile using a simple arctan model, representing the interseismic strain accumulation. Our slip rates compare well with current geologic estimates, which suggests that the present-day velocity field is representative of long-term motions. We find that the transform is a zone of high strain rate up to 80 km wide that is straighter than the SAF and has an overall trend closer to the relative plate motion vector than the SAF. Most sections of the SAF take up less than half of the total slip rate, and slip is transferred from one part of the system to another in a way that suggests that the SAF should not be considered as a unique locator of the plate boundary. Up to half of the total displacement takes place on faults outside the high strain rate zone, distributed over several hundred kilometers on either side. Our findings substantiate previous suggestions that the transform has the characteristics of a macroscopic ductile shear zone cutting the continental lithosphere, around which stress and strain rate decrease on a length scale controlled by the length of the transform.

1. Introduction

[2] Geodetically determined velocities across California allow us to define in detail the distribution of strain rate in the Pacific–North American plate boundary zone (Figure 1). This distribution has two intriguing aspects. First, it is not everywhere centered on the San Andreas Fault (SAF), which is commonly regarded as the surface trace of the plate boundary. Second, it shows a central zone of high strain rate, several tens of kilometers wide, with a quasi-exponential decrease in rate on either side. This can be visualized directly from a 1-D velocity profile across the boundary (Figure 2), which shows a central zone of high velocity gradient (corresponding to high strain rate) and a sigmoidal decrease in the velocity gradient on either side. The question we discuss in this paper is what controls this distribution of velocity and strain rate.
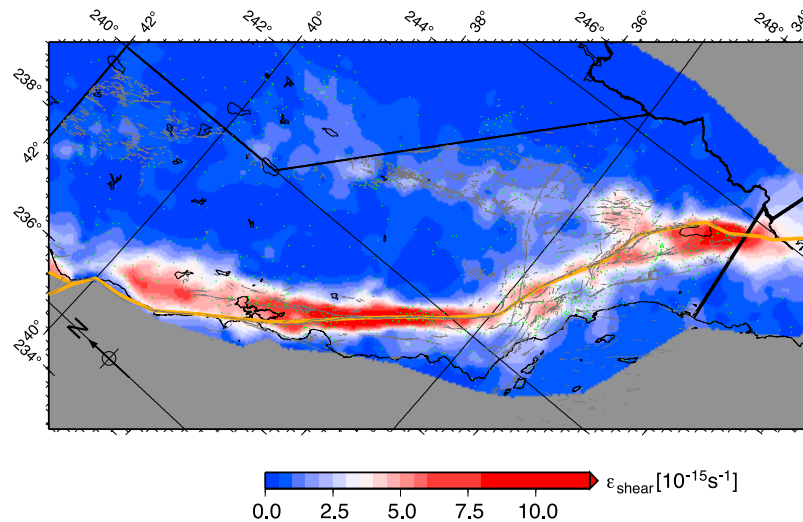
Figure 1. Scalar strain rate (second invariant of the 2-D strain rate tensor) calculated using velocities interpolated from the PBO MIT Joint Network (November 2009) and *Kreemer and Hammond*'s [2007] GPS compilations, plotted on an oblique Mercator projection (see *Platt et al.* [2008] for details on the interpolation method). Note that the zone of highest strain rate does not everywhere coincide with the surface trace of the SAF, is straighter than the SAF, and has an overall trend that is closer to the plate motion vector than the SAF.

[3] The simple answer is that it represents strain localization. This is a property of most solids at relatively low temperatures and results from microstructural damage caused by deformation, which weakens the material and causes it to deform more rapidly. Strain localization is essential for plate tectonics: numerical models of mantle convection fail to reproduce comprehensive plate-like behavior in the thermal boundary layer unless the material shows a significant degree of strain localization [*Bercovici*, 2003]. The details of the strain rate distribution should therefore inform us about the
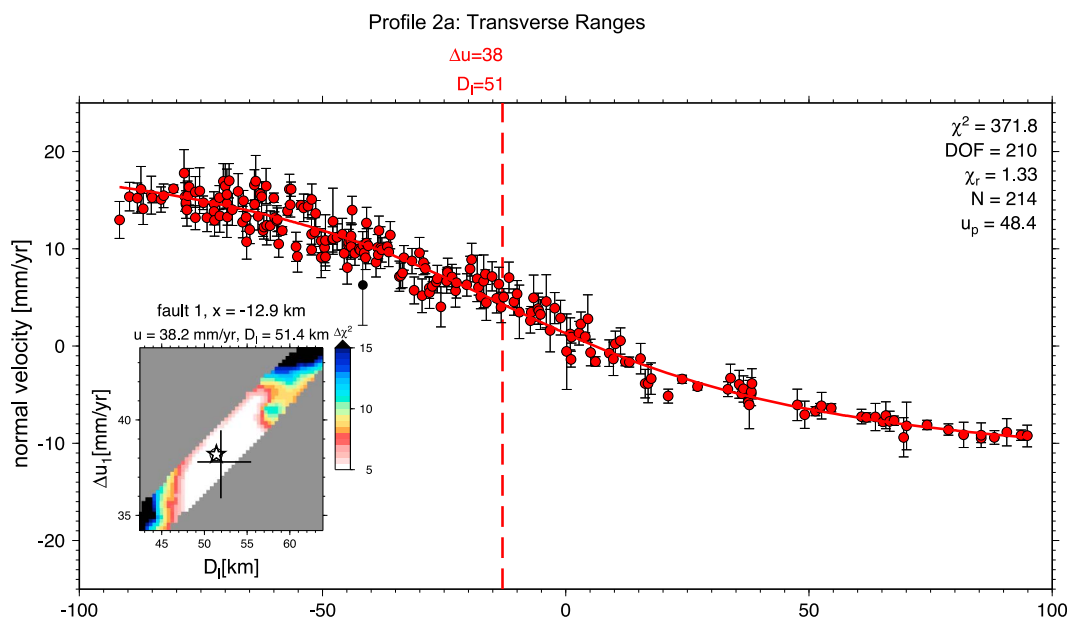
Figure 2. Velocity profile across southern California, interpreted in terms of elastic flexure around a single fault. A good fit to the profile is obtained, but this interpretation requires a flexural parameter of 50 km, far greater than is likely given the high heat flow and low lithospheric thickness accepted for this region. The location of the fault does not coincide with any known structure, lying 15 km east of the surface trace of the San Andreas Fault, and several other major active faults are present in this profile.

material properties of the lithosphere and the process of weakening. Two end-member approaches to interpreting the data have been suggested.

[4] 1. One mechanically simple approach is to treat the velocities as resulting from the flexure of elastic plates bounding an intermittently locked dislocation [e.g., *Savage and Burford*, 1973]. By adjusting the elastic thickness and the velocity difference between the plates, it is possible to fit the data remarkably well (Figure 2). *Smith and Sandwell* [2003], for example, demonstrated that geodetic data could be fit by varying these two parameters in 12 successive profiles along the full length of the SAF. There are, however, some disadvantages to this approach. As noted above, the zone of maximum accumulation of shear strain does not everywhere correspond to the SAF, or indeed to any single fault (Figure 2). Second, a literal interpretation of elastic dislocation theory for a single fault implies that the fault in question is locked down to as much as ~50 km, far below the depth to which faults are seismogenic in a region of relatively thin lithosphere and high heat flow such as California (Figure 2). Last, it is well established from geological evidence that there are many active faults within the transform system, some of which have slip rates comparable to the SAF. Elastic dislocation models have therefore been improved by incorporating more complex rheologies [e.g., *Hetland and Hager*, 2005; *Pollitz*, 2001; *Lundgren et al.*, 2009] and by including multiple faults with more realistic, 3-D geometry [e.g., *Meade and Hager*, 2005]. Implicit in these models is the idea that the velocity distribution is the envelope of the elastic profiles around multiple faults with variable slip rates and locking depths, but none of them address the question as to why the slip rates on these faults should vary systematically so as to produce the observed velocity distribution.

[5] 2. The second approach is to treat the transform as a shear zone that applies a stress boundary condition to the plates on either side [e.g., *Platt et al.*, 2008]. The transform has a length of order 10^3 km and applies a load to plates with dimensions of order 10^4 km, so the stress decays away from the boundary. *England et al.* [1985] showed that if the lithosphere behaves as a thin sheet with power law viscosity, then the velocity and the strain rate will decay away from the boundary on a length scale that is related to the length of the boundary and the power law exponent [e.g., *Whitehouse et al.*, 2005].

[6] These two approaches are very different but not irreconcilable. There is little doubt that the upper crust is a brittle-elastic solid and that the geodetically determined velocity gradients around individual faults largely reflect interseismic elastic strain accumulation. On larger spatiotemporal scales, however, strain rates likely reflect the bulk mechanical properties of the lithosphere as a whole. The question is to what extent the geodetically observed velocity distribution constitutes a proxy for the long-term pattern of permanent deformation. Here we fit velocities using classic elastic dislocation theory [*Savage and Burford*, 1973], not because this is necessarily the right mechanical description but because it allows us to straightforwardly extract slip rate estimates on sets of faults across the whole plate boundary. We then compare our geodetic estimates to geologic estimates of slip rates on longer time scales and show that they are in general consistent with the longer-term rates. The overall velocity distribution at present may therefore give us useful information about the bulk, long-term mechanical properties of the lithosphere.

2. Methods

[7] Several methods have been used for analyzing and interpreting geodetic data. *Bourne et al.* [1998] suggested that where there is an array of subparallel faults, as in southern California, the velocities of the intervening fault blocks correspond to the average velocity of the ductilely deforming lithosphere beneath them. Their argument depends on the assumption that the brittle upper crust has negligible strength compared to the underlying ductile layer. This is questionable: a wide range of evidence suggests that in tectonically active areas such as California much of the strength of the continental lithosphere resides within the brittle upper crust [*Sibson*, 1983; *Maggi et al.*, 2000; *Townend*, 2006]. The conclusions of *Bourne et al.* [1998] are still valid, however, if we assume that all the faults have the same resistance to motion. The net force exerted by the bounding faults on each block is then zero, and force balance then requires the net traction on the base of the block to be zero. This will only be true if the velocity of the block is the same as the average velocity of the ductile substrate beneath it. Note that this argument does not imply that the ductile substrate is necessarily driving the blocks. The assumption that the faults have the same resistance to motion is unlikely to be strictly true, but it would be difficult to make the case that the velocity distribution across California is entirely controlled by strength differences among the different faults.

[8] *Roy and Royden* [2000a, 2000b] suggested that surface velocities are a result of the diffusion of deformation above a master fault at depth, mediated by the ductile lower crust. This model depends on the assumption that the plate boundary is defined by a discrete slip surface in the lithospheric mantle, which appears to be at odds with evidence from shear wave splitting for zones of deformation tens to hundreds of kilometers wide in the mantle beneath major transform zones [*Herquel et al.*, 1999; *Rümpker et al.*, 2003; *Savage et al.*, 2004; *Baldock and Stern*, 2005; *Becker et al.*, 2006]. The model of *Roy and Royden* [2000a, 2000b] also predicts a time-dependent widening of the zone of surface deformation. Geologic evidence suggests, however, that the transform zone has been about the same width at least since it adopted its present trajectory across southern California [*Atwater and Stock*, 1998; *Dickinson and Wernicke*, 1997; *McQuarrie and Wernicke*, 2005].

[9] Most workers now agree that in order to determine slip rates on faults some way has to be found of estimating the interseismic elastic strain accumulation. The simplest approach is the elastic dislocation model [*Savage and Burford*, 1973]. This is based on the assumption of a semi-infinite elastic layer with a slip surface that terminates upward at a depth (known as the locking depth), which controls the length scale of the elastic flexure in the medium above the fault. This produces an interseismic velocity profile described by $v = -v_0 \arctan [x/D_l]/\pi$, where v_0 is the total velocity difference across the fault, x is distance normal to the fault, and D_l is the flexural parameter or locking depth. The model has the advantage of simplicity, although it has little resemblance to the real Earth.

[10] The viscoelastic coupling model [e.g., *Savage and Prescott*, 1978; *Thatcher*, 1983; *Pollitz*, 2001; *Hetland and Hager*, 2006] assumes intermittent slip on a fault in an elastic layer that overlies a homogeneous viscoelastic medium. Slip on the fault induces short-term elastic strain in the underlying medium, which then relaxes, loading the overlying layer until the fault slips again. The resulting surface velocity profile is time dependent, and its variability depends on the ratio between the recurrence time and the Maxwell time of the viscoelastic medium. This concept has been used to extract mantle viscosities, as well as slip rates on faults. It has limitations in that it assumes vertically and laterally homogeneous mechanical properties and linear viscous rheology. In the real world, strike-slip faults are likely to be underlain by ductile shear zones with fundamentally different mechanical properties from the surrounding rocks [e.g., *Bürgmann and Dresen*, 2008] and nonlinear relationships between stress and strain rate. We note that some workers have attempted to address these issues [e.g., *Reches et al.*, 1994; *Pollitz*, 2001; *Freed and Bürgmann*, 2004; *Hetland and Hager*, 2005], but it is also true that the viscoelastic model cannot be fully tested until we have geodetic observations through the full seismic cycle on a fault.

[11] The mechanical significance of the flexural parameter in elastic models is uncertain. It is commonly assumed to represent the depth to the brittle-ductile transition or to the base of the seismogenic layer. In the real Earth, however, it seems more likely that it would represent the effective thickness of the flexed layer that accommodates the interseismic elastic strain [*Chéry*, 2008]. In this sense, it is analogous to the elastic thickness of the lithosphere obtained from vertical loading [e.g., *Watts*, 1992], although the values may be different for strike-slip versus vertical loading.

[12] Where fault spacing is less than a few times the flexural parameter, it becomes difficult to separate the overlapping velocity profiles and to apportion slip rates correctly to the different faults. An increase in the flexural parameter for one of the faults will result in more of the velocity profile being attributed to slip on that fault and less on the others. Hence, there is a trade-off between the flexural parameter and slip rate for each fault, which substantially increases the real uncertainties in both estimates [*Freymueller et al.*, 1999; *Schmalzle et al.*, 2006; *d'Alessio et al.*, 2005]. This is a possible explanation for some of the variety in geodetic estimates for slip rates.

[13] Recent attempts to quantify slip rates on faults in the San Andreas Transform system using geodetic data have therefore applied a variety of sophisticated approaches, including block models incorporating numerous faults, some of which also utilize stress or geologic slip rate inferences [e.g., *Bennett et al.*, 1996; *Meade and Hager*, 2005; *Becker et al.*, 2005; *McCaffrey*, 2005], and viscoelastic models [e.g., *Pollitz et al.*, 2008; *Smith-Konter and Sandwell*, 2009]. These models have the advantage that they can build in complex 3-D geometries, rotations, and variations in slip rate on the faults, but it can be difficult to see the relationship between data and model results or to discover the possible causes of apparent discrepancies between the modeled slip rates and geologic data, which in some cases are extreme [e.g., *Meade and*

Hager, 2005]. Moreover, significant trade-offs among model parameters persist [*Becker et al.*, 2005].

[14] We have chosen to use a simple, one-dimensional approach based on the classic elastic dislocation model of *Savage and Burford* [1973]. Our method is comparable to the block model method [e.g., *Bennett et al.*, 1996; *Meade and Hager*, 2005] in that we assume rigid blocks bounded by faults, but the 1-D analysis allows immediate visual inspection of the fit of the model to the data and of the trade-offs between slip rates on the various faults. It also allows us to trace slip rates through the system in a straightforward way, identifying where slip is being transferred laterally from one part of the system to another. We believe the relative transparency of our approach will be of value to others, working with both geodetic and geologic data, in comparing our results with theirs.

[15] Our justification for using the classic elastic dislocation model is that most major faults in California have seismic cycles that are short relative to the likely viscous relaxation time for the lithospheric mantle, and they are all well into, or late in, their current cycle. Under these conditions the velocity distribution in the upper crust predicted by the viscoelastic coupling model is geometrically similar to the elastic dislocation model [e.g., *Hetland and Hager*, 2006]. After about 40% of the way through the seismic cycle, the value of the flexural parameter that we determine using the classical method should be greater than the thickness of the elastic layer if the viscoelastic model is applicable. Surprisingly, the values we obtain are all relatively small, which suggests that this does not present a problem. Our aim is to extract long-term slip rate data, and the main analytical problem we face is the overlap of the elastic profiles between adjacent faults. Application of more sophisticated techniques, with their larger number of free parameters, does not necessarily help with this problem.

[16] The elastic dislocation model of *Savage and Burford* [1973] was developed for faults of infinite length. Application of this model could result in erroneous slip rates near the terminations and junctions of faults, but these effects are unlikely to be significant in the central sections of long strike-slip faults. We have tried as far as possible to choose areas far from major fault junctions and terminations.

[17] In conclusion, we feel the use of the classical elastic dislocation model to 1-D profiles is appropriate for the purpose of this study, although it does not mean that we subscribe to the mechanical description of the lithosphere on which it is based.

3. Velocity Analysis

[18] We analyze the data along six swaths normal to the trend of the transform (Figure 3) and present them in the form of velocity profiles along these swaths (Figures 4 and 5). We assume that slip rate is conserved along faults between their intersections, so swaths that do not cross any intersections should produce unique and reproducible values for the slip rates. Our method does not identify permanent deformation between the faults or slip on faults that we have not identified: these components of the deformation field are collapsed onto the faults that we have identified, and our slip rates may therefore be too high. Comparison with geologically inferred slip rates, however, suggests that this problem is not serious, with a few exceptions that we discuss below.

[19] We use the high-quality GPS velocities from EarthScope PBO (November 2009 MIT solution) which were merged with the compilation of continuous and campaign GPS data from *Kreemer and Hammond* [2007] in order to fill in some gaps in the PBO coverage, arriving at 2858 data total, out of which 1954 are in our study region. We remove some outliers by requiring the quoted velocity uncertainties to be smaller than 10 mm/yr and select the datum with the smaller error bar if entries are located closer than 1.5 km, leaving us with 1562 data. The velocity data were each rotated into a half plate motion reference frame [cf. *Wdowinski et al.*, 2007] for visualization and analysis purposes, using the geodetically determined Euler pole for the Pacific plate relative to stable North America from *Meade and Hager* [2005]. We verified that our results are robust with respect to simple shifts in reference frame by alternatively rotating each data set into its own best fit half plate motion frame before merging.

[20] In a first step, we find the best fitting model solution to the velocity profiles, using all original projected data (shown in black on the profiles). After testing several approaches to invert for the best model fit, we used the Simplex algorithm by *Nelder and Mead* [1965] to optimize the flexural parameters and fault locations for several test cases while solving for slip rates using a nonnegative least squares inversion for each given geometry (requiring dextral slip on all faults). Flexural parameters were limited to a maximum of 15 km
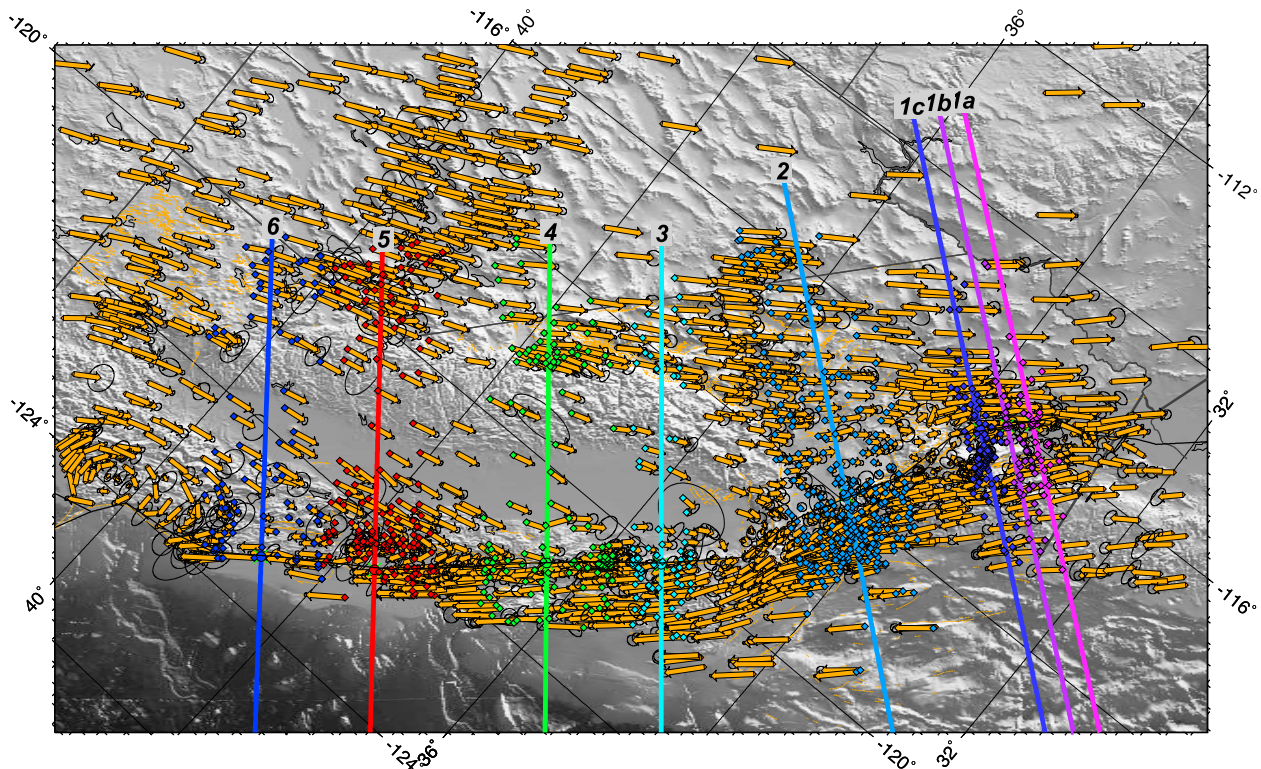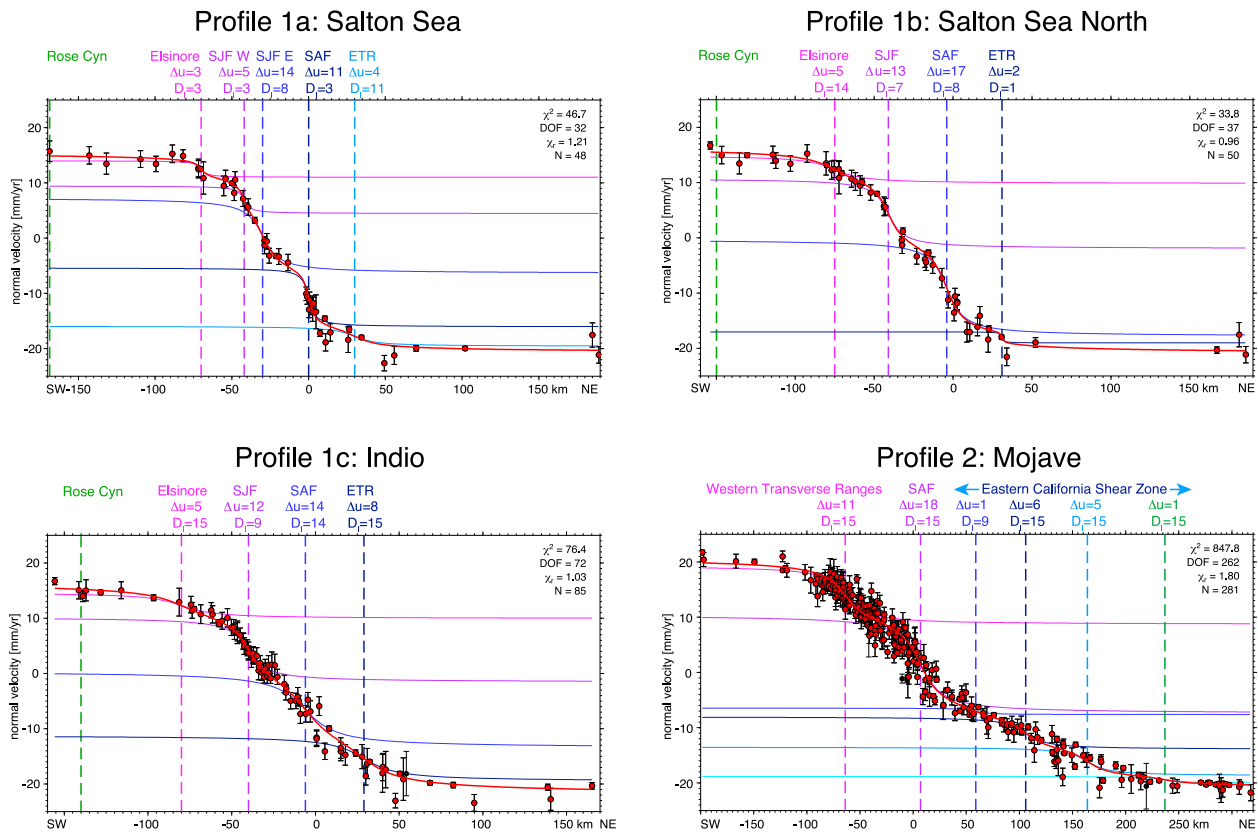
Figure 3. Map of California, showing the locations of our velocity profiles, together with the velocity data set used in this paper. The velocities are plotted in a reference frame that is half the geodetically inferred Pacific–North America plate motion using the Euler pole from *Meade and Hager* [2005].

for the models shown, but we tested that results allowing for values up to 30 km yielded consistent slip rates. We then redo each initial fit using only the data that are within 6 mm/yr of our best fit to avoid obvious outliers (the data actually used are shown in red on the profiles); this step only leads to minor readjustments. To evaluate the trade-off between model parameters we then compute ~20,000 auxiliary solutions from a Monte Carlo simulation of Gaussian errors of the GPS data. We determine bounds on the parameter ranges assuming that $\Delta\chi^2$ statistics [e.g., *Press et al.*, 1993, p. 693f] hold.

[21] In performing a weighted least squares inversion, it became clear that some profiles and their misfit statistics were dominated in places by individual PBO velocities with very small quoted error bars. While continuous GPS is, of course, expected to yield more reliable results than the campaign data included in the *Kreemer and Hammond* [2007] compilation, we feel that there are some systematic mismatches in the error estimates, and we therefore arbitrarily scaled up the PBO uncertainties by a factor of 2. In general, slip rate estimates do not

differ by more than ~1 mm/yr for those scaled data compared to those with original PBO uncertainties, but we feel that the misfit statistics for the merged data are more meaningful in the scaled up uncertainty models which will be discussed below.

[22] Fault locations were prescribed in all the inversions we discuss below. Our choice as to which faults to include is based on a trial and error approach, as follows. We identified major, active fault zones in each profile and then ran inversions to check whether the slip rate and flexural parameters could be moderately well constrained. Faults for which no slip rate could be assigned within uncertainties were eliminated. We also ran inversions where the algorithm itself was to pick fault locations, in order to identify faults we had not taken into account, which had not been correctly located, or which are dipping so that the flexural signal is offset from the surface trace. In some cases, in the ECSZ, for example, where active faults are known to exist but the algorithm was not able to locate them or assign slip rates with confidence, we made choices based on the accepted

Figure 4. Velocity profiles from southern California (see Figure 3 for locations), showing the horizontal component of velocity parallel to the Pacific–North America plate motion vector, with fault locations and slip rate interpretations. Fault locations were prescribed; flexural parameters D_l were obtained by inversion but were constrained to lie between 1 and 15 km, and slip rates Δu were fit by means of nonnegative least squares (ensuring dextral slip on all faults). ETR in profiles 1a and 1c and Western Transverse Ranges and Fort Irwin Fault System at +164 km in profile 2 represent rotating panels of E-W trending sinistral faults for which we estimate the net dextral slip rate. See Tables 1a and 1b for details of the values and ranges; see the auxiliary material for plots showing the trade-off between slip rate and locking depth for all faults.

locations of the faults; these cases are highlighted below.

4. Results

[23] The results of our analysis are displayed in Figures 4 and 5, and the inferred slip rates and flexural parameters are tabulated in Tables 1a and 1b. In the auxiliary material, we show plots indicating the range of well-fitting solutions for the slip rate and flexural parameter for each fault.[1] On many of these plots, the well-fitting models define a narrow band with positive slope, indicating a trade-off between flexural parameter and slip rate. The higher the flexural parameter for a particular fault, the more of the velocity profile as a whole is treated

as part of the flexural response to motion on that fault. This means that adjacent faults would have to have lower slip rates and in most cases lower flexural parameters. Much of the uncertainty in our determinations arises from this trade-off [cf. *Freymueller et al.*, 1999]. Where the faults are closely spaced, the uncertainty on the individual determinations becomes unacceptably large, and we have chosen to group two or more faults together, with substantially reduced uncertainty on the combined slip rate.

[24] Creeping faults, such as the San Juan Bautista sector of the SAF and the Hayward Fault, are associated with little or no buildup of elastic strain [*Johanson and Bürgmann*, 2005; *Schmidt et al.*, 2005], so the flexural parameter is not meaningful. We set the parameter to 1 km for the purposes of determining the slip rate on the Hayward Fault.
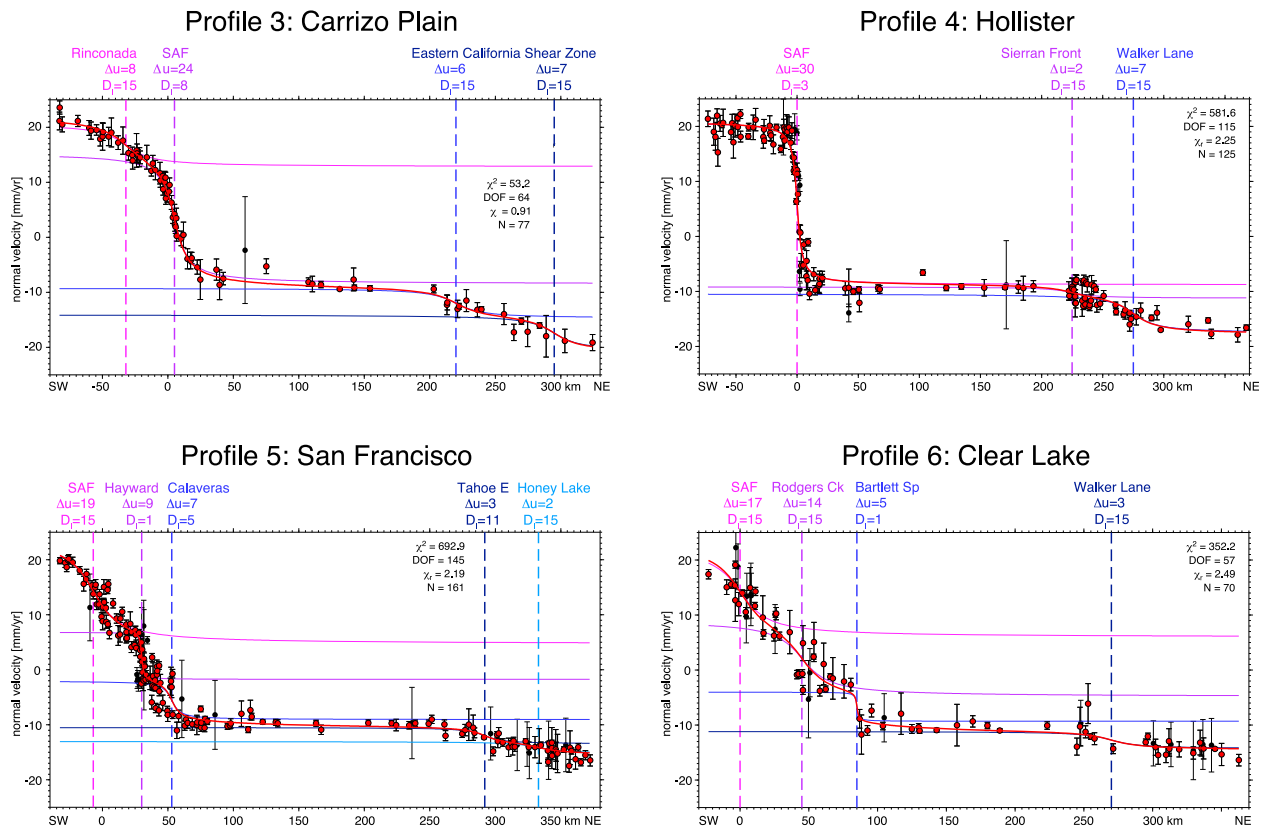
Figure 5. Velocity profiles from central and northern California (see Figure 3 for locations and caption to Figure 4 for details). D_l for the creeping section of the Hayward Fault in profile 5 was prescribed at 1 km.

[25] Some of the swaths, such as profiles 1a–1c and 2, cross panels of roughly E-W trending faults with sinistral or reverse sense, such as the Transverse Ranges and the Fort Irwin area in the NE Mojave Desert. We modeled these panels as individual dextral faults in order to determine the rate of dextral shear across them: the flexural parameter in these cases clearly has no significance, but the integrated rate of dextral shear is reasonably robust. Dextral shear is transmitted across these panels by a combination of sinistral slip on the faults and clockwise vertical axis rotation (Figure 6), as indicated by the large paleomagnetically determined rotations from these areas [*Carter et al.*, 1987; *Hornafius et al.*, 1986; *Luyendyk*, 1991; *Luyendyk et al.*, 1980; *Schermer et al.*, 1996].

5. Comparison With Geologic Estimates

[26] A comparison of our slip rate estimates with current geologic estimates is presented in Table 2. Most of the geologic estimates are taken from the

values tabulated by *Bird* [2007]. This compilation eliminates estimates that are based partly or wholly on geodetic data, which is essential if our comparison is to be valid. The values we quote are the upper and lower bounds of the 95% confidence range of the probability density function as calculated by *Bird* [2007] from multiple geologic esti-

Table 1a. Velocity Data for Profiles 1–6[a]

	Δu for Curve	u(west)	u(east)	u(plate)	u0
Profile 1a	35.9	15.3	−20.6	47.6	−2.7
Profile 1b	37.3	16.4	−20.9	47.6	−2.2
Profile 1c	38.5	16.6	−21.9	47.6	−2.6
Profile 2	42.0	20.8	−21.1	48.4	−0.2
Profile 3	43.8	22.4	−21.4	49.2	0.5
Profile 4	38.8	21.0	−17.9	49.2	1.5
Profile 5	40.0	24.3	−15.8	49.5	4.3
Profile 6	38.9	24.0	−14.9	49.4	4.5

[a]Δu is the total velocity change across the profile, u(west) and u (east) are the velocities at either end of the profile relative to the half plate motion reference frame, u(plate) is the relative plate velocity at the location of the profile, and u0 is the velocity at the midpoint of the modeled curve.

**Table 1b.** Slip Rate and Flexural Parameter Estimates for Profiles 1–6[a]

Fault	x	Best du	Minimum du	Median du	Maximum du	Best Dl	Minimum Dl	Median Dl	Maximum Dl
Profile 1a									
Elsinore	−70.0	3.0	0.0	2.9	6.6	3.1	1.0	3.4	15.0
SJF W	−42.0	5.0	2.0	5.0	17.9	3.1	1.0	2.9	15.0
SJF E	−30.0	13.6	4.0	13.4	24.3	8.1	1.0	7.9	15.0
SAF	0.0	10.7	6.7	10.7	15.6	3.2	1.0	3.2	7.4
ETR	30.0	3.6	1.2	3.4	5.4	10.7	1.0	10.9	15.0
Profile 1b									
Elsinore	−75.0	5.1	1.1	4.8	7.3	14.1	1.0	14.9	15.0
SJF	−41.0	12.7	8.7	12.8	20.1	7.1	2.7	7.1	15.0
SAF	−4.0	17.5	13.4	17.3	23.6	8.0	3.4	7.9	15.0
ETR	31.0	2.0	0.0	2.1	4.5	1.0	1.0	1.0	15.0
Profile 1c									
Elsinore	−80.0	4.7	1.7	4.5	6.2	15.0	1.0	15.0	15.0
SJF	−40.0	11.7	8.0	12.6	19.1	8.6	2.8	9.5	15.0
SAF	−6.0	13.8	6.4	13.0	16.9	14.1	2.7	14.8	15.0
ETR	29.0	8.3	5.9	8.1	11.0	15.0	5.7	15.0	15.0
Profile 2									
WTR	−64.0	10.6	10.6	10.6	11.0	15.0	14.9	15.0	15.0
SAF	7.0	17.8	16.8	17.8	18.0	15.0	12.9	15.0	15.0
Helendale	59.0	1.2	0.7	1.2	1.9	9.3	1.0	9.3	15.0
Blackwater	106.0	5.9	4.7	5.9	6.8	15.0	8.2	15.0	15.0
Fort Irwin	164.0	5.2	3.7	5.2	5.7	15.0	4.6	15.0	15.0
Stateline	237.0	1.2	0.8	1.2	1.8	15.0	1.0	15.0	15.0
Profile 3									
Rinconada	−32.0	7.9	3.8	7.8	9.6	15.0	1.0	15.0	15.0
SAF	5.0	23.8	21.8	23.9	27.2	7.7	5.1	7.8	11.1
Owens Valley	220.0	5.5	3.7	5.5	6.9	15.0	1.0	15.0	15.0
Fish Creek	295.0	6.7	3.8	6.7	9.4	15.0	1.0	15.0	15.0
Profile 4									
SAF	0.0	29.6	29.2	29.6	30.0	2.9	2.5	2.9	3.4
Sierra Front	225.0	2.1	1.7	2.1	2.7	15.0	9.5	15.0	15.0
Walker Lane	275.0	7.2	6.0	7.2	7.4	14.9	8.9	14.9	15.0
Profile 5									
SAF	−7.0	19.3	18.6	19.3	19.5	15.0	13.8	15.0	15.0
Hayward	30.0	8.6	8.3	8.6	8.9	1.0	1.0	1.0	1.0
Calaveras	53.0	7.0	6.3	7.0	8.0	4.8	1.9	4.8	8.8
Tahoe E	292.0	3.0	2.2	3.0	4.0	10.6	1.0	10.7	15.0
Honey Lake	333.0	2.2	0.9	2.1	2.8	15.0	1.0	15.0	15.0
Profile 6									
SAF	0.0	16.5	14.0	16.5	16.9	15.0	11.2	15.0	15.0
Rodgers Ck	32.0	13.9	13.2	13.9	15.1	15.0	13.7	15.0	15.0
Bartlett Sp	72.0	5.3	5.3	5.3	5.7	1.0	1.0	1.0	4.2
ECSZ	270.0	3.2	2.6	3.2	3.3	15.0	1.0	15.0	15.0

[a]x is the fault location in the profile (zero is the map trace of the SAF), du is slip rate, and Dl is the flexural parameter. Best fit, minimum, median, and maximum values are shown for du and Dl. These values and ranges are shown graphically in the trade-off plots in the auxiliary material.

mates. Where only one geologic estimate is available, we quote that value with the uncertainty, or the upper or lower bounds, as given by the original author. We note that the real uncertainties on individual geologic estimates are in general likely to be significantly larger than the quoted uncer-

tainties, a point discussed in detail, for example, by *Behr et al.* [2010].

[27] Overall, our geodetic estimates fit well with the geologic estimates, supporting our contention that the present-day velocity field is a useful proxy
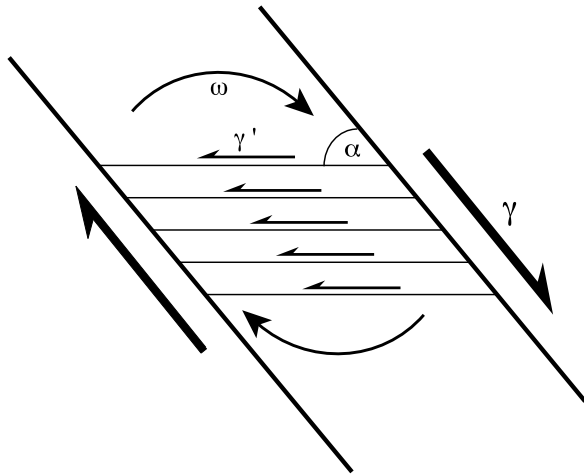
Figure 6. Diagram showing how dextral shear can be accommodated by a combination of slip on a set of sinistral faults accompanied by clockwise rotation. If γ is the rate of shear in the dextral fault zone and α is the angle of the sinistral faults to the plane of bulk simple shear, the slip rate on the sinistral faults is $\gamma' = -\gamma \cos2\alpha$, the rate of rotation of the faults and fault blocks is $\omega = \gamma(1 - \cos2\alpha)/2$, and the fault blocks have to stretch internally at a rate $e = (\gamma \sin2\alpha)/2$ to maintain compatibility with their surroundings.

for long-term rate of deformation in California. The main exceptions are some sections of the San Andreas Fault system itself and the Mojave Desert region, discussed below. A justification for our simplified modeling arises from the observation that our results are consistent along different sections of the main strands of the system. For example, our estimate for the total transform-parallel slip rate on the Eastern California Shear Zone (ECSZ) and adjacent areas of the Basin and Range province is 14.6 ± 1.3 mm/yr over the four northern profiles, north of the Garlock Fault. This gives us a high degree of confidence in treating this as a long-term rate of displacement across this region, which then places constraints on slip rates farther south. Another example is our estimate of a total of 16–19 mm/yr slip on the Coast Ranges faults east of the San Andreas Fault in profiles 5 and 6. The consistency of this result, even though the uncertainties on the individual faults are large, suggests that it is a reliable estimate of the long-term displacement rate in the northern Coast Ranges. Similarly, our estimate for the total slip rate within Salinia west of the SAF is 9–11 mm/yr, consistent with the total slip rate in southern California west of the San Jacinto Fault (11–13 mm/yr). In section 6 we discuss our slip rate estimates in the context of the overall slip rate budget for the transform system (Figure 7). This allows us to evaluate the areas

Table 2. Comparison of Slip Rates Based on Our Geodetic Analysis With Geologic Estimates[a]

	Profile 6			
	Offshore	SAF	RC/M	Bartlett Sp
Geodetic analysis	1–2	14–17	13–15	5–6
Geologic estimate		18.4 ± 2.4	11–18	3.4 ± 0.7
	Profile 5			
	H-SG	SAF	Hayward	Calaveras
Geodetic analysis	0–1	19–20	8–9	6–8
Geologic estimate	1–9	13.8 ± 0.9	8 ± 0.3	5–13
	Profile 4			
	H-SG	SAF		
Geodetic analysis	3–4	29–30		
Geologic estimate	7.2 ± 1.1	33.4 ± 3.0		
	Profile 3			
	H-SG	Rinconada	SAF	ECSZ
Geodetic analysis	2–4	4–10	22–27	11–14
Geologic estimate	3.1 ± 3.1	1–5	35.6 ± 0.4	11.0 ± 0.4
	Profile 2			
	Offshore	WTR	SAF	ECSZ
Geodetic analysis	3–4	11	17–18	12–14
Geologic estimate			28.5 ± 1.8	6.2 ± 1.9
	Mean Profile 1			
	Elsinore	SJF	SAF	ETR
Geodetic analysis	3–5	12–19	11–18	2–8
Geologic estimate	5.8 ± 1.3	13.6 ± 1.3	18.4 ± 1.9	

[a]H-SG, Hosgri–San Gregorio Fault; RC-M, Rodgers Creek Ma'acama Fault; WTR, Western Transverse Ranges; ETR, Eastern Transverse Ranges; ECSZ, Eastern California Shear Zone. Geodetic values shown for profile 1 show the range in best fit solutions from the three swaths (1a, 1b, and 1c). Ranges for geodetic slip rates on individual faults from the other profiles are the minimum and maximum solutions from Tables 1a and 1b. Ranges for composite systems (WTR, ECSZ, and offshore structures) are estimated from the velocity profiles and the ranges on the adjacent major faults. Geologic estimates from *Bird* [2007], *Lindvall and Rockwell* [1995], *Oskin et al.* [2008], *Petersen and Wesnousky* [1994], and *Shen-Tu et al.* [1999]. Uncertainties where quoted are from *Bird* [2007] based on multiple determinations; ranges are from determinations by individual authors.
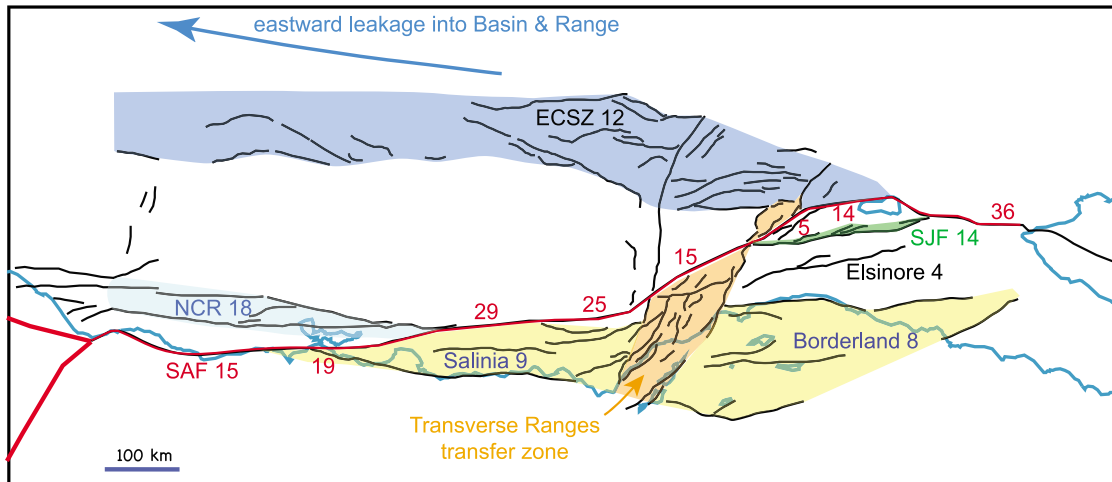
	offshore	SAF	RC/M	Bartlett Sp	NCR total	ECSZ	B&R	TOTAL
Profile 6	3	15	7	11	18	3	10	49
Profile 5	1	19	Hayward 9	Calaveras 6	15	5	9	50
Profile 4	4	29				9	7	49
Profile 3	2	Rinconada 7		SAF 25		12	3	49
Profile 2	3	WTR 12			SAF 15	15	3	48
Profile 1	8	Elsinore 4	SJF 14		SoSAF 14	4	3	48

Figure 7. Slip rate budget for California, showing major faults and bands of grouped faults, with our interpreted slip rates. (bottom) The slip rates in tabular form for each profile, including the additional slip rate at the ends of each profile needed to bring the total to the Pacific–North America relative plate velocity. The color bands show schematically how the slip is transferred along strike. (top) Map showing in simplified form how the slip is distributed among the different parts of the system, together with their linkages.

where our results differ significantly from geologic estimates and from other estimates based on geodetic data.

6. Slip Rate Budget for the San Andreas Transform System

6.1. Profile 1

[28] Profile 1 (Salton Sea) was split into three subsets (profiles 1a–1c) because there was so much scatter of the velocities near the SAF that we were unable to carry out a meaningful inversion. On the individual subprofiles an automated inversion picks the SAF and San Jacinto Fault reliably, with the SAF slightly west of its surface trace (Tables 1a and 1b); the Elsinore Fault is picked on profiles 1b and 1c only. The Rose Canyon fault is at the west end of the profile, and additional slip is being taken up on offshore faults such as the San Clemente fault, so we can only determine the cumulative slip rate on the Borderland faults (8 mm/yr) by using the total Pacific–North American plate motion (Figure 7). At the eastern end we have modeled deformation in the Eastern Transverse Ranges (ETR) by a single fault 30 km east of the SAF: deformation in this region is in fact accommodated by a rotating panel of E-W sinistral faults, including the Pinto Mountain, Blue Cut, and Chiriaco faults [Carter et al., 1987].

[29] For the purposes of our slip rate budget we have averaged the results from the three profiles. We estimate subequal slip rates of 14 ± 3 mm/yr on the San Jacinto and southern San Andreas faults. These are within uncertainties of the geologic estimates, but our slip rate for the SAF is lower than previous geodetic estimates: e.g., 23.5 mm/yr [Meade and Hager, 2005], 23 mm/yr [Becker et al.,

2005] (based on GPS only), and 25 mm/yr [*Fialko*, 2006]. This is at least partly because we distinguish about 5 mm/yr of dextral shear east of the SAF in the Eastern Transverse Ranges. This displacement has been incorporated within the elastic strain profile of the SAF by other workers. It is, however, an important component of the process by which displacement is transferred northward off the southern SAF into the Mojave Desert region.

[30] A total of 14 mm/yr has to be transferred from the Salton Sea profile into the Mojave Desert region (Figure 7). How this happens is unclear as no throughgoing faults have been identified. In addition to displacement being transferred through the ETR, some is clearly being transferred along the network of faults that slipped during the Landers 1992 M_w 7.3 earthquake, and some may be being transferred by a combination of reverse faulting and clockwise rotation across the San Bernadino Mountains. Our analysis does not provide information on the details of this process. The slip rate budget does, however, imply that slip on the SAF through San Gorgonio Pass and on the San Bernardino segment is slow (~5 mm/yr but with a large uncertainty), as suggested by *Meade and Hager* [2005] and *Becker et al.* [2005]. Our budget also implies that ~12 mm/yr of displacement is transferred off the San Jacinto Fault northward onto the SAF around Cajon Pass.

6.2. Profile 2

[31] In profile 2 (Mojave) only the SAF can be located reliably; the automated inversion places it 7 km east of its surface trace, implying that it dips west in this area. We modeled deformation in the Western Transverse Ranges (WTR) by a single fault aligned with the trace of the Newport-Inglewood Fault, and we specified the locations of four faults in the Mojave Desert (see below). Our slip rate estimate for the SAF is 17–18 mm/yr. This is in agreement with the geodetic estimate by *Meade and Hager* [2005], but it is substantially lower than geologic estimates, quoted by *Bird* [2007] as 28.5 ± 1.8 mm/yr. Bird's estimate is largely based on a detailed analysis by *Matmon et al.* [2005], who carried out a careful analysis of the uncertainties in both the offset measurements and ages of a series of offset fans all derived from the same source at Pallet Creek. Their final estimate, based on a Monte Carlo analysis of the combined uncertainties, is 30 ± 10 mm/yr, where the quoted uncertainty is 1σ. The discrepancy may therefore not be as large as suggested by Bird's estimate with its very low

uncertainty. This is, however, a kinematically very complex area, with significant discrepancies between geologic and geodetic slip rate estimates across the Mojave Desert, and displacement being transferred by a combination of thrust faulting and vertical axis rotation through the Transverse Ranges. Further consideration of profile 2, therefore, requires discussion of both these regions.

6.3. Mojave Desert and the Garlock Fault

[32] The velocity profile across the Mojave Desert (profile 2) is approximately linear, with a velocity difference of 12–14 mm/yr over 200 km. Twelve mm/yr of this velocity difference is transferred into the ECSZ farther north (see profile 3); the remainder is apparently transferred back onto the SAF (see below).

[33] The linear velocity gradient is most easily explicable in terms of slip at low rates on a large number of faults, but the geodetic data are insufficient to locate the active faults or to resolve the slip rates on them. To illustrate a possible solution, we show four faults on the profile. Three of these are dextral faults observed on the ground (the Helendale, Blackwater, and Stateline faults), and we located another at +164 km east of the SAF to model the clockwise-rotating panel of E-W trending sinistral faults around Fort Irwin in the NE Mojave Desert [*Schermer et al.*, 1996]. Our estimated slip rates on the individual faults have little significance, but the total rate of displacement of 12–14 mm/yr is robust. This conclusion is controversial as *Oskin et al.* [2008] suggested that the sum total of the geologically estimated dextral slip rates on faults in the Mojave Desert region amounts to 6.2 ± 1.9 mm/yr. They suggest that the discrepancy between the geologically and geodetically determined strain rates is a result of a temporary increase in elastic strain rate accumulation related to earthquake clustering in the Mojave Desert region.

[34] As discussed below (profile 3), our estimate of 12 mm/yr of dextral shear across the ECSZ north of the Garlock Fault is well supported by other geodetic studies as well as neotectonic analyses. Simple mass balance considerations require that this rate of displacement must be transferred southward in some form across the Garlock Fault into the Mojave Desert. If *Oskin et al.* [2008] are correct that the geologic slip rate has not exceeded 8 mm/yr for at least the last 30,000 years, this requires the accumulation of at least 120 m of dextral elastic displacement within the Mojave Desert section of

the ECSZ, equivalent to a deficit of approximately 15 magnitude 8 earthquakes during this period. An alternative explanation is that some of the other four to six faults that cross the Mojave Desert [*Dokka and Travis*, 1990] may have slip rates of around 1 mm/yr that have not yet been detected geologically.

[35] An implication of the geodetically observed shear strain rate across the Garlock Fault is that the fault itself must be rotating clockwise. The fault is not cut by any of the dextral faults in the ECSZ, all of which lose their displacement rates as they approach the fault [*Oskin and Iriondo*, 2004; *Oskin et al.*, 2007]. The regional dextral shear strain across the Garlock Fault must therefore be accommodated by a combination of sinistral slip and clockwise rotation (Figure 6). The rate of rotation ω of a fault (or other) plane at an angle α to the plane of bulk simple shear is $\omega = \gamma (1 - \cos 2\alpha)/2$, where γ is the rate of simple shear. The average angle between the main section of the Garlock Fault and the plate boundary is 72°. Dextral shear across the ECSZ is distributed over 130 km normal to the transform direction, giving a shear strain rate of 9.2×10^{-8}/yr, so the fault and its surroundings must rotate clockwise at 8.3×10^{-8} radians/yr, or 4.8°/Myr. The slip rate on the Garlock Fault implied by this process is 7.4 mm/yr sinistrally, which is within the range of geologically determined rates for the Garlock Fault [*McGill et al.*, 2009].

[36] About 2 of the total 14 mm/yr displacement rate across the Mojave Desert is apparently not transferred onto the ECSZ farther north but is transferred back onto the SAF. The northwestern Mojave appears in fact to be converging with the southern Sierra Nevada and Great Valley. The effect is small and may be a result of far-field elastic strain associated with the SAF (which would increase our estimate of the slip rate on the SAF). It is noteworthy, however, that the second largest earthquake in California during the 20th century was the M_w 7.3 Kern County earthquake [*Bawden*, 2001]. This was caused by reverse motion on the E-W trending White Wolf Fault in the southern Sierra Nevada. We suggest therefore that about 2 mm/yr of displacement is being transferred between the NW Mojave and SAF via the White Wolf Fault and related structures in the southern Sierra Nevada and Tehachapi Mountains.

6.4. Transverse Ranges

[37] The Transverse Ranges comprise a zone of E-W trending sinistral and reverse faults that cut right across the transform zone in the region of the big bend in the SAF. None of the NW trending dextral faults except the SAF itself continue through the Transverse Ranges, and their displacements are reorganized and transferred in complex ways across it. Much of this displacement transfer is achieved on reverse faults, which act to transfer dextral slip westward from southern California into the Coast Ranges farther north. One example is the Cucamonga–Sierra Madre fault system along the southern front of the San Gabriel Mountains, which transfers about 2 mm/yr of NW directed displacement off the San Jacinto Fault westward and beneath the Transverse Ranges and onto the San Andreas Fault north of Cajon Pass. Other dextral faults in southern California (Elsinore, Newport-Inglewood, and the offshore borderland faults) transfer displacement via the reverse faults of the western Transverse Ranges onto the Rinconada and Hosgri–San Gregorio Faults in coastal central California.

[38] We modeled the deformation in the western Transverse Ranges with a single fault aligned with the trace of the Newport-Inglewood Fault, but this is simply a device to obtain the total rate of distributed dextral shear in this region, which we estimate at 11 mm/yr. This deformation is not accommodated on right-slip faults, and the slip rate on the Newport-Inglewood Fault itself, which lies south of the Transverse Ranges, is below our detection limit.

[39] The overall NW directed dextral shear across the western Transverse Ranges has the effect of rotating all the E-W trending structures in a clockwise sense, as discussed above for the case of the Garlock Fault. Approximately 11 mm/yr of displacement rate is distributed across a zone ~150 km wide, corresponding to a rate of shear strain of 7.3×10^{-8}/yr. The Transverse Ranges trend on average at 50° to the plate boundary, so this rate of shear strain will rotate the structures at 2.5°/Myr on average. Clockwise rotation of the western Transverse Ranges over Neogene time is well documented [*Luyendyk et al.*, 1985], and the present-day strain rate field indicates that this rotation is continuing. *McCaffrey* [2005] has argued that there is no ongoing rotation of the western Transverse Ranges, on the basis that no components of velocity normal to the transform trend are detectable. This argument is based on the assumption that the rotating blocks are roughly equant and are rotating independently of their surroundings. The actual structure of the Transverse Ranges consists of a series of E-W trending fault slices bounded by a combination of reverse and sinistral faults. The combination of
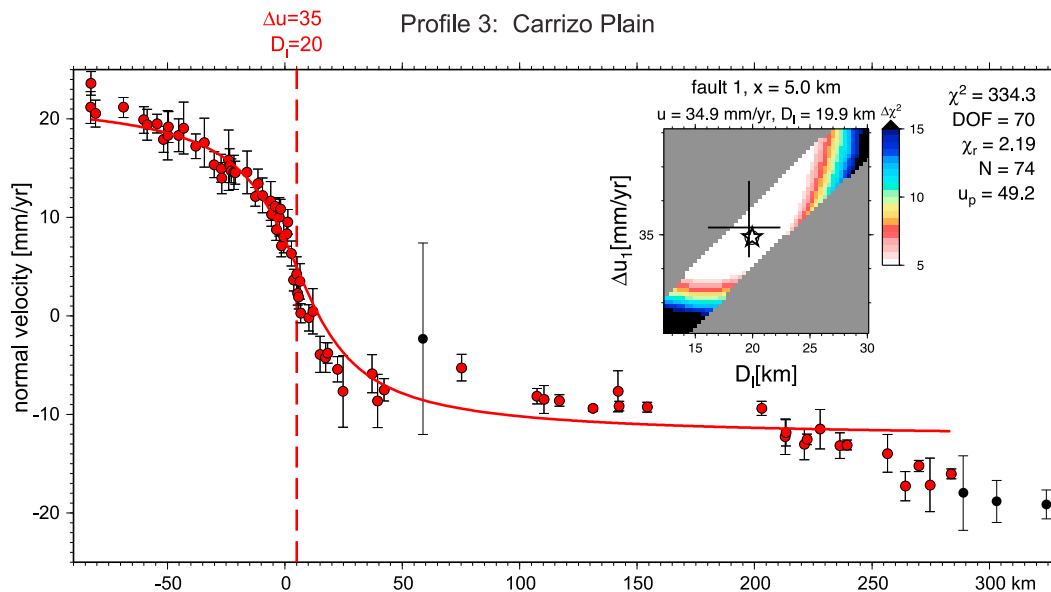
Figure 8. Best fit velocity profile for a slip rate of 36 mm/yr on the Carrizo Plain section of the SAF, as suggested by *Meade and Hager* [2005]. Compare with profile 3 in Figure 5.

sinistral slip and clockwise rotation is kinematically equivalent to dextral shear, and no significant components of velocity normal to the transform trend are required (Figure 6). Note that the rotations mean that dip-slip displacement rates on the reverse faults will change along strike, decreasing westward on the south side of the Transverse Ranges and increasing westward on the north side.

6.5. Profile 3

[40] In profile 3 (Carrizo Plain) the SAF and the Rinconada Fault are reliably located by an automated inversion; the SAF is located 5 km east of its surface trace. We specified locations for the Owens Valley and Fish Creek faults. No slip rate could be detected within uncertainty on any other fault. Our estimate for the slip on this section of the SAF is 22–27 mm/yr, compared to the geologic estimate of 35.6 ± 0.4 mm/yr [*Bird*, 2007]. Our estimate is also significantly lower than other geodetic estimates: e.g., 35.9 mm/yr by *Meade and Hager* [2005] and 33 mm/yr by *Becker et al.* [2005]. Part of the reason for the discrepancy is that in contrast to other analyses we assign 8 mm/yr to the Rinconada Fault. This is high compared to geologic estimates (1–5 mm/yr), and if this is reduced, the slip rate on the SAF would increase correspondingly, although this reduces the goodness of fit. A slip rate of >27 mm/yr, however, would also require a significant reduction of the slip rate in the ECSZ, and the fit to the velocity profile as a whole becomes very poor (Figure 8). Our estimate of the total slip rate across

the ECSZ in profile 3 is 11–14 mm/yr, which compares well with the sum of the geologically determined slip rates on the Owens Valley Fault, the East Inyo Fault Zone, and the Northern Death Valley Fault Zone [*Lee et al.*, 2009] and also to other geodetic determinations [*Dixon et al.*, 2000; *McClusky et al.*, 2001; *Bennett et al.*, 2003]. We regard this rate as robust, and it places a significant constraint on the total possible slip rate on the Carrizo Plain section of the SAF.

[41] It appears therefore that there may be a real discrepancy between geologic and geodetic slip rate estimates for the Carrizo Plain section. Evaluation of the reasons for this lies outside the scope of this paper, however.

6.6. Profile 4

[42] In profile 4 (Hollister), a free inversion locates the SAF, the Sierran frontal fault system, and the Walker Lane. Our estimated slip rate for the SAF is 29–30 mm/yr, which is within uncertainty of the geologic estimate (33 ± 3 mm/yr). The increased rate relative to that in the Carrizo Plain section probably reflects transfer of slip from the Rinconada Fault farther south. The small value for the flexural parameter (2 km) reflects the fact that the fault is creeping in this area. The slip rate in the ECSZ in this profile is 9 mm/yr, compared to 12 mm/yr farther south, reflecting progressive transfer of slip into the NW Basin and Range, a process that continues in profiles 5 and 6.

6.7. Profile 5

[43] Profile 5 (San Francisco) presents problems because the close spacing of the faults in the Bay Area makes it difficult to isolate their individual contributions to the overall velocity profile. A free inversion locates the SAF and Hayward Fault, but the SAF is located 7 km west of its surface trace. We have used this location, but it probably reflects the effect of the Hosgri–San Gregorio Fault, which lies a few kilometers to the west, and our estimated slip rate of 19–20 mm/yr for the SAF likely incorporates slip on both faults. This may explain why our estimate is high compared to the geologic estimate of 13.8 ± 1 mm/yr [*Bird*, 2007]. We set the flexural parameter for the Hayward Fault to 1 km, reflecting the fact that it is creeping and therefore does not contribute elastic strain buildup. We prescribed the location of the Calaveras Fault, and we modeled deformation in the ECSZ with a fault located on the east side of the Tahoe graben and another at Honey Lake. The uncertainties on our estimates on individual faults are large, but the combined slip rate estimate of 15 mm/yr on the Hayward and Calaveras faults is reasonably consistent with the combined slip rate of 18 mm/yr on equivalent faults in profile 6.

[44] Comparable slip rates are estimated by *d'Alessio et al.* [2005], using a block model with prescribed locations for all the faults. The differences between their results and ours can be largely attributed to the fact that with the exception of the Calaveras Fault, we have not ascribed slip rates to faults that we could not locate from the geodetic data.

6.8. Profile 6

[45] In profile 6 (Clear Lake) the GPS data sampling is too poor to automatically pick faults. We specified locations for the SAF, the Rodgers Creek Fault, and the Bartlett Springs Fault. Our slip rate estimates have large uncertainties but are reasonably consistent with the geologic estimates. They confirm the impression given by the strain rate map (Figure 1) that a large part of the total displacement rate lies inshore of the SAF, as noted by *Freymueller et al.* [1999].

7. Significance of the Velocity Field for the Location and Nature of the Plate Boundary

[46] Our analysis suggests that the geodetically determined velocity field in California, which largely reflects interseismic elastic strain, is a reasonably good proxy for the long-term permanent deformation related to the plate boundary. Apparent discrepancies between geodetic and geological estimates of slip rate appear not to be systematic and may result from unrecognized uncertainties in both methods of determination. We can therefore make a number of statements based on the pattern of strain rate seen in Figure 1 and on our analysis of the slip rate budget in Figure 7.

[47] First, the lithospheric transform is a zone of high strain rate several tens of kilometers wide that is not everywhere centered on the surface trace of the San Andreas Fault. In southern California it is ~60 km wide, overlapping both the SAF and the San Jacinto Fault, and the SAF lies close to its eastern margin. In northern California it is ~80 km wide, and the SAF lies at its extreme western margin. In central California it is narrower and centered on the SAF: this partly reflects the extreme weakness of the fault in this region, which localizes upper crustal deformation to a greater extent than elsewhere. Overall, the zone of high strain rate is straighter than the SAF and has a trend that is closer to the plate motion vector than the SAF.

[48] A second feature, brought out by our slip rate budget (Figure 7), is that the SAF commonly takes up less than half of the total slip rate, and slip is transferred from one part of the system to another in a way that suggests that the SAF should not be considered as a unique locator of the plate boundary, even at the surface. In particular, most of the slip rate on the southern strand of the SAF in the Coachella Valley passes into the ECSZ, and only ~6 mm/yr makes its way onto the central strand of the SAF in the Great Valley, most of the remainder being transferred from the San Jacinto Fault. In the San Francisco Bay area, about half the slip rate from the central strand of the SAF is progressively transferred onto the Calaveras, Hayward, and related faults in the northern Coast Ranges.

8. Significance of the Strain Rate Distribution for Strain Localization in the Lithosphere

[49] The geodetically defined strain rate distribution at the surface largely reflects interseismic, elastic smearing of the longer-term slip on the individual faults. Our analysis removes the elastic effects, leaving a stepped pattern reflecting the long-term slip rates on the faults in upper crust.

Below the seismogenic layer, deformation is continuous and more distributed and in general is likely to become progressively less localized with depth in the Earth [e.g., *Vauchez and Tomassi*, 2003]. Strain localization is controlled in part by rock composition, water content, and strain rate but most importantly by temperature. Faults therefore pass down into ductile shear zones that broaden with depth. Major strike-slip faults that have been exhumed from depths of 20–30 km are found to form shear zones between 10 and 40 km wide [*Corsini et al.*, 1991; *Pili et al.*, 1997; *West and Hubbard*, 1997; *Vauchez and Tomassi*, 2003], and several shear wave splitting studies suggest that these shear zones may be 40–100 km wide or more in the upper mantle [*Herquel et al.*, 1999; *Moore et al.*, 2002; *Rümpker et al.*, 2003; *Savage et al.*, 2004; *Wilson et al.*, 2004; *Baldock and Stern*, 2005]. The width of these shear zones is comparable to the spacing between the surface faults within the zone of high strain rate defined by geodesy. The San Jacinto and San Andreas faults in southern California, for example, are 30–40 km apart, and the San Andreas, Rodgers Creek, and Bartlett Springs faults in the northern California Coast Ranges are each separated by a similar distance. These faults, which are discrete structures at the surface, may therefore merge into a single broad shear zone in the deep crust or upper mantle.

[50] We therefore have three different descriptions of the strain rate distribution: the short-term pattern of elastic strain accumulation at the surface, the longer-term pattern of slip on upper crustal faults, and the distribution of ductile shear at depth. None of these is more true than the others; they simply reflect the varying behavior of the lithosphere on different time scales and at different depths. Taken together, however, they justify describing the transform zone as a lithospheric shear zone, with an overall distribution of strain rate that can be inferred from the geodetic data. This leads us to our last point.

[51] Except in southernmost California, just about half the total plate boundary displacement takes place outside the high strain rate zone that we have identified, and produces deformation in the ECSZ, the Southern California Borderland, the central and western Transverse Ranges, and the central Coast Ranges including offshore areas of central California. We therefore distinguish two mechanical components to the overall plate boundary zone. One is a zone of high strain rate, several tens of kilometers wide, expressed at the surface by a series of linked major faults including the SAF. This is likely to correspond at depth to a major ductile shear zone. The second component is a broad region of plate boundary related deformation extending for as much as 200 km on either side of the high-strain zone, with an overall decrease of strain rate away from it. As discussed above, this may be related to quasi-exponential decrease of stress and strain rate away from the transform zone into the surrounding plates [*England et al.*, 1985; *Whitehouse et al.*, 2005; *Platt et al.*, 2008], on a length scale related to the length of the transform. Part of this deformation has been deflected into the ECSZ by the presence of a relatively rigid block of lithosphere centered on the Sierra Nevada [*Whitehouse et al.*, 2005]. The boundary condition for this deformation is the vertically averaged shear stress within the lithospheric shear zone, which is in turn controlled by the rheology of the material in the shear zone, its width, and the imposed rate of displacement.

9. Conclusions

[52] We use a simple and transparent method to invert geodetic data for slip rates on faults in California. This gives results that are largely in agreement with geologic slip rate estimates, and we construct a slip rate budget for the San Andreas system that is consistent with Pacific–North America relative plate motion. Integrated slip rates for discrete sections of the system, such as the ECSZ, the northern Coast Ranges faults, and the Salinia–Southern California Borderland, are consistent along strike, giving us additional confidence in our results. We therefore conclude that the present-day geodetically defined velocities are a reasonable proxy for the longer-term pattern of permanent deformation in California. This then leads us to infer that the position and width of the band of high strain rate through California reflects the real character of the lithospheric transform. It is a zone up to 80 km wide, centered west of the SAF in southern California and east of it in the north of the Bay Area. It is straighter than the SAF and has a trend that is closer to the plate motion vector than the SAF. The width of this zone may approximate the width of a ductile shear zone in the deep lithosphere, and the distribution of slip on the surface faults within the zone may reflect the strain rate distribution at depth.

[53] Only about half the total plate motion is accommodated by this zone of high strain rate. The remainder is distributed over a much broader region, with strain rate and total displacement

decreasing away from the high strain rate zone. The distribution of stress and strain rate in this broader zone may be governed by the length scales concept for deformation of a thin viscous sheet, as originally articulated by *England et al.* [1985].

Acknowledgments

References

Atwater, T., and J. Stock (1998), Pacific–North America plate tectonics of the Neogene southwestern United States: An update, in *Integrated Earth and Environmental Evolution of the Southwestern United States: The Clarence A. Hall, Jr. Volume*, edited by W. G. Ernst and C. A. Nelson, pp. 393–420, Bellwether, Columbia, Md.

Baldock, G., and T. Stern (2005), Width of mantle deformation across a continental transform: Evidence from upper mantle (Pn) seismic anisotropy measurements, *Geology*, *33*, 741–744, doi:10.1130/G21605.1.

Bawden, G. W. (2001), Source parameters for the 1952 Kern County earthquake, California: A joint inversion of leveling and triangulation observations, *J. Geophys. Res.*, *106*, 771–785, doi:10.1029/2000JB900315.

Becker, T. W., J. L. Hardebeck, and G. Anderson (2005), Constraints on fault slip rates of the southern California plate boundary from GPS velocity and stress inversions, *Geophys. J. Int.*, *160*, 634–650, doi:10.1111/j.1365-246X. 2004.02528.x.

Becker, T. W., V. Schulte-Pelkum, D. L. Blackman, J. B. Kellogg, and R. J. O'Connell (2006), Mantle flow under the western United States from shear wave splitting, *Earth Planet. Sci. Lett.*, *247*, 235–251, doi:10.1016/j.epsl.2006. 05.010.

Behr, W. M., et al. (2010), Uncertainties in slip rate estimates for the Mission Creek strand of the southern San Andreas fault at Biskra Palms Oasis, *Geol. Soc. Am. Bull.*, *122*(9–10), 1360–1377, doi:10.1130/B30020.s.

Bennett, R. A., W. Rodi, and R. E. Reilinger (1996), Global Positioning System constraints on fault slip rates in Southern California and northern Baja, Mexico, *J. Geophys. Res.*, *101*, 21,943–21,960, doi:10.1029/96JB02488.

Bennett, R. A., B. P. Wernicke, N. A. Niemi, and A. M. Friedrich (2003), Contemporary strain rates in the northern Basin and Range province from GPS data, *Tectonics*, *22*(2), 1008, doi:10.1029/2001TC001355.

Bercovici, D. (2003), The generation of plate tectonics from mantle convection, *Earth Planet. Sci. Lett.*, *205*, 107–121, doi:10.1016/S0012-821X(02)01009-9.

Bird, P. (2007), Uncertainties in long-term geologic offset rates of faults: General principles illustrated with data from California and other western states, *Geosphere*, *3*, 577–595, doi:10.1130/GES00127.1.

Bourne, S. J., P. C. England, and B. Parsons (1998), The motion of crustal blocks driven by flow of the lower lithosphere and implications for slip rates of continental strike-slip faults, *Nature*, *391*, 655–659, doi:10.1038/35556.

Bürgmann, R., and G. Dresen (2008), Rheology of the lower crust and upper mantle: Evidence from rock mechanics, geodesy, and field observations, *Annu. Rev. Earth Planet. Sci.*, *36*, 531–567, doi:10.1146/annurev.earth.36.031207. 124326.

Carter, J. N., B. P. Luyendyk, and R. Terres (1987), Neogene clockwise tectonic rotation of the eastern Transverse Ranges, California, suggested by paleomagnetic vectors, *Geol. Soc. Am. Bull.*, *98*, 199–206, doi:10.1130/0016-7606(1987) 98<199:NCTROT>2.0.CO;2.

Chéry, J. (2008), Geodetic strain across the San Andreas fault reflects elastic plate thickness variations (rather than fault slip rate), *Earth Planet. Sci. Lett.*, *269*, 352–365, doi:10.1016/j. epsl.2008.01.046.

Corsini, M., A. Vauchez, C. Archanjo, and E. F. J. de Sá (1991), Strain transfer at continental scale from a transcurrent shear zone to a transpressional fold belt: The Patos-Seridó system, northeastern Brazil, *Geology*, *19*, 586–589, doi:10.1130/0091-7613(1991)019<0586:STACSF>2.3. CO;2.

d'Alessio, M. A., I. A. Johanson, R. Bürgmann, D. A. Schmidt, and M. H. Murray (2005), Slicing up the San Francisco Bay Area: Block kinematics and fault slip rates from GPS-derived surface velocities, *J. Geophys. Res.*, *110*, B06403, doi:10.1029/2004JB003496.

Dickinson, W. R., and B. P. Wernicke (1997), Reconciliation of San Andreas discrepancy by a combination of interior Basin and Range extension and transrotation near the coast, *Geology*, *25*, 663–665, doi:10.1130/0091-7613(1997) 025<0663:ROSASD>2.3.CO;2.

Dixon, T. H., M. Miller, F. Farina, H. Wang, and D. Johnson (2000), Present-day motion of the Sierra Nevada block and some implications for the Basin and Range province, North American Cordillera, *Tectonics*, *19*, 1–24, doi:10.1029/ 1998TC001088.

Dokka, R. K., and C. J. Travis (1990), Late Cenozoic strike-slip faulting in the Mojave Desert, California, *Tectonics*, *9*, 311–340, doi:10.1029/TC009i002p00311.

England, P., G. Houseman, and L. Sonder (1985), Length scales for continental deformation in convergent, divergent, and strike-slip environments: Analytical and approximate solutions for a thin viscous sheet model, *J. Geophys. Res.*, *90*, 3551–3557, doi:10.1029/JB090iB05p03551.

Fialko, Y. (2006), Interseismic strain accumulation and the earthquake potential on the southern San Andreas fault system, *Nature*, *441*, 968–971, doi:10.1038/nature04797.

Freed, A. M., and R. Bürgmann (2004), Evidence of power-law flow in the Mojave desert mantle, *Nature*, *430*, 548–551, doi:10.1038/nature02784.

Freymueller, J. T., M. H. Murray, P. Segall, and D. Castillo (1999), Kinematics of the Pacific–North America plate boundary zone, northern California, *J. Geophys. Res.*, *104*, 7419–7441, doi:10.1029/1998JB900118.

Herquel, G., P. Tapponnier, G. Wittlinger, J. Mei, and S. Danian (1999), Teleseismic shear wave splitting and lithospheric anisotropy beneath and across the Altyn Tagh fault, *Geophys. Res. Lett.*, *26*, 3225–3228, doi:10.1029/1999GL005387.

Hetland, E. A., and B. H. Hager (2005), Postseismic and interseismic displacements near a strike-slip fault: A two-dimensional theory for general linear viscoelastic rheologies, *J. Geophys. Res.*, *110*, B10401, doi:10.1029/2005JB003689.

Hetland, E. A., and B. H. Hager (2006), Interseismic strain accumulation: Spin-up, cycle invariance, and irregular rup-

ture sequences, *Geochem. Geophys. Geosyst.*, *7*, Q05004, doi:10.1029/2005GC001087.

Hornafius, J. S., B. P. Luyendyk, R. R. Terres, and M. J. Kammerling (1986), Timing and extent of rotation in the western Transverse Ranges, California, *Geol. Soc. Am. Bull.*, *97*, 1476–1487, doi:10.1130/0016-7606(1986)97<1476: TAEONT>2.0.CO;2.

Johanson, I. A., and R. Bürgmann (2005), Creep and quakes on the northern transition zone of the San Andreas fault from GPS and InSAR data, *Geophys. Res. Lett.*, *32*, L14306, doi:10.1029/2005GL023150.

Kreemer, C., and W. C. Hammond (2007), Geodetic constraints on areal changes in the Pacific-North America plate boundary zone: What controls Basin and Range extension?, *Geology*, *35*, 943–947, doi:10.1130/G23868A.1.

Lee, J., D. Stockli, L. A. Owen, R. C. Finkel, and R. Kislitsyn (2009), Exhumation of the Inyo Mountains, California: Implications for the timing of extension along the western boundary of the Basin and Range Province and distribution of dextral fault slip rates across the eastern California shear zone, *Tectonics*, *28*, TC1001, doi:10.1029/2008TC002295.

Lindvall, S. C., and T. K. Rockwell (1995), Holocene activity of the Rose Canyon fault zone in San Diego, California, *J. Geophys. Res.*, *100*, 24,121–24,132, doi:10.1029/95JB02627.

Lundgren, P., E. A. Hetland, Z. Liu, and E. Fielding (2009), Southern San Andreas–San Jacinto fault system slip rates estimated from earthquake cycle models constrained by GPS and interferometric synthetic aperture radar observations, *J. Geophys. Res.*, *114*, B02403, doi:10.1029/2008JB005996.

Luyendyk, B. P. (1991), A model for Neogene crustal rotations, transtension, and transpression in southern California, *Geol. Soc. Am. Bull.*, *103*, 1528–1536, doi:10.1130/0016-7606(1991)103<1528:AMFNCR>2.3.CO;2.

Luyendyk, B. P., M. J. Kamerling, and R. Terres (1980), Geometric model for Neogene crustal rotations in southern California, *Geol. Soc. Am. Bull.*, *91*, 211–217, doi:10.1130/0016-7606(1980)91<211:GMFNCR>2.0.CO;2.

Luyendyk, B. P., M. J. Kamerling, R. R. Terres, and J. S. Hornafius (1985), Simple shear of southern California during Neogene time suggested by paleomagnetic declinations, *J. Geophys. Res.*, *90*, 12,454–12,466, doi:10.1029/JB090iB14p12454.

Maggi, A., J. A. Jackson, D. McKenzie, and K. Priestley (2000), Earthquake focal depths, effective elastic thickness, and the strength of the continental lithosphere, *Geology*, *28*, 495–498, doi:10.1130/0091-7613(2000)28<495:EFDEET>2.0.CO;2.

Matmon, A., D. P. Schwartz, R. C. Finkel, S. Clemmens, and T. Hanks (2005), Dating offset fans along the Mojave section of the San Andreas fault using cosmogenic ^{26}Al and ^{10}Be, *Geol. Soc. Am. Bull.*, *117*, 795–807, doi:10.1130/B25590.1.

McCaffrey, R. (2005), Block kinematics of the Pacific–North American plate boundary in the southwestern United States from inversion of GPS, seismological, and geologic data, *J. Geophys. Res.*, *110*, B07401, doi:10.1029/2004JB003307.

McClusky, S. C., S. C. Bjornstad, B. H. Hager, R. W. King, B. J. Meade, M. M. Miller, F. C. Monastero, and B. J. Souter (2001), Present day kinematics of the eastern California shear zone from a geodetically constrained block model, *Geophys. Res. Lett.*, *28*, 3369–3372, doi:10.1029/2001GL013091.

McGill, S. F., S. G. Wells, S. K. Fortner, H. A. Kuzma, and J. D. McGill (2009), Slip rate of the western Garlock fault, at Clark Wash, near Lone Tree Canyon, Mojave Desert, California, *Geol. Soc. Am. Bull.*, *121*, 536–554.

McQuarrie, N., and B. P. Wernicke (2005), An animated reconstruction of southwestern North America since 35 Ma, *Geosphere*, *1*, 147–172, doi:10.1130/GES00016.1.

Meade, B. J., and B. H. Hager (2005), Block models of crustal motion in southern California constrained by GPS measurements, *J. Geophys. Res.*, *110*, B03403, doi:10.1029/2004JB003209.

Moore, M., P. England, and B. Parsons (2002), Relation between surface velocity field and shear wave splitting in the South Island of New Zealand, *J. Geophys. Res.*, *107*(B9), 2198, doi:10.1029/2000JB000093.

Nelder, J. A., and R. Mead (1965), A simplex method for function minimization, *Comput. J.*, *7*, 308–313.

Oskin, M., and A. Iriondo (2004), Large magnitude transient strain accumulation on the Blackwater fault, Eastern California shear zone, *Geology*, *32*, 313–316, doi:10.1130/G20223.1.

Oskin, M., L. Perg, D. Blumentritt, S. Mukhopadhyay, and A. Iriondo (2007), Slip rate of the Calico fault: Implications for geologic versus geodetic rate discrepancy in the Eastern California Shear Zone, *J. Geophys. Res.*, *112*, B03402, doi:10.1029/2006JB004451.

Oskin, M., L. Perg, E. Shelef, M. Strane, E. Gurney, B. Singer, and X. Zhang (2008), Elevated shear zone loading rate during an earthquake cluster in eastern California, *Geology*, *36*, 507–510, doi:10.1130/G24814A.1.

Petersen, M. D., and S. G. Wesnousky (1994), Fault slip rates and earthquake histories for active faults in southern California, *Bull. Seismol. Soc. Am.*, *84*, 1608–1649.

Pili, E., Y. Ricard, J.-M. Lardeaux, and S. M. F. Sheppard (1997), Lithospheric shear zones and mantle-crust connections, *Tectonophysics*, *280*, 15–29, doi:10.1016/S0040-1951(97)00142-X.

Platt, J. P., B. J. P. Kaus, and T. W. Becker (2008), The mechanics of continental transforms: An alternative approach with applications to the San Andreas system and the tectonics of California, *Earth Planet. Sci. Lett.*, *274*, 380–391, doi:10.1016/j.epsl.2008.07.052.

Pollitz, F. F. (2001), Viscoelastic shear zone model of a strike-slip earthquake cycle, *J. Geophys. Res.*, *106*, 26,541–26,560, doi:10.1029/2001JB000342.

Pollitz, F. F., P. McCrory, J. Svarc, and J. Murray (2008), Dislocation models of interseismic deformation in the western United States, *J. Geophys. Res.*, *113*, B04413, doi:10.1029/2007JB005174.

Press, W. H., S. A. Teukolsky, W. T. Vetterling, and B. P. Flannery (1993), *Numerical Recipes in C: The Art of Scientific Computing*, 1020 pp., Cambridge Univ. Press, Cambridge, U. K.

Reches, Z., G. Schubert, and C. Anderson (1994), Modeling of periodic great earthquakes on the San Andreas Fault: Effects of nonlinear crustal rheology, *J. Geophys. Res.*, *99*, 21,983–22,000, doi:10.1029/94JB00334.

Roy, M., and L. H. Royden (2000a), Crustal rheology and faulting at strike-slip boundaries: 2. Effects of lower crustal flow, *J. Geophys. Res.*, *105*, 5599–5613, doi:10.1029/1999JB900340.

Roy, M., and L. H. Royden (2000b), Crustal rheology and faulting at strike-slip boundaries: 1. An analytical model, *J. Geophys. Res.*, *105*, 5583–5597, doi:10.1029/1999JB900339.

Rümpker, G., T. Ryberg, G. Bock, and D. S. Group (2003), Boundary-layer mantle flow under Dead Sea transform

inferred from seismic anisotropy, *Nature*, *425*, 497–501, doi:10.1038/nature01982.

Savage, J., and R. Burford (1973), Geodetic determination of relative plate motion in central California, *J. Geophys. Res.*, *78*, 832–845, doi:10.1029/JB078i005p00832.

Savage, J. C., and W. H. Prescott (1978), Asthenospheric readjustment and the earthquake cycle, *J. Geophys. Res.*, *83*, 3369–3376, doi:10.1029/JB083iB07p03369.

Savage, M. K., K. M. Fischer, and C. E. Hall (2004), Strain modelling, seismic anisotropy and coupling at strike-slip boundaries: Applications in New Zealand and the San Andreas fault, *Geol. Soc. Spec. Publ.*, *227*, 9–39.

Schermer, E. R., B. P. Luyendyk, and S. Cisowski (1996), Late Cenozoic structure and tectonics of the northern Mojave Desert, *Tectonics*, *15*, 905–932, doi:10.1029/96TC00131.

Schmalzle, G., T. Dixon, R. Malservisi, and R. Govers (2006), Strain accumulation across the Carrizo segment of the San Andreas Fault, California: Impact of laterally varying crustal properties, *J. Geophys. Res.*, *111*, B05403, doi:10.1029/2005JB003843.

Schmidt, D. A., R. Bürgmann, R. M. Nadeau, and M. A. d'Alessio (2005), Distribution of aseismic slip rate on the Hayward fault inferred from seismic and geodetic data, *J. Geophys. Res.*, *110*, B08406, doi:10.1029/2004JB003397.

Shen-Tu, B., W. Holt, and A. J. Haines (1999), Deformation kinematics in the western United States determined from Quaternary fault slip rates and recent geodetic data, *J. Geophys. Res.*, *104*, 28,927–28,955, doi:10.1029/1999JB900293.

Sibson, R. H. (1983), Continental fault structure and the shallow earthquake source, *J. Geol. Soc.*, *140*, 741–767, doi:10.1144/gsjgs.140.5.0741.

Smith, B., and D. Sandwell (2003), Coulomb stress accumulation along the San Andreas Fault system, *J. Geophys. Res.*, *108*(B6), 2296, doi:10.1029/2002JB002136.

Smith-Konter, B., and D. Sandwell (2009), Stress evolution of the San Andreas fault system: Recurrence interval versus locking depth, *Geophys. Res. Lett.*, *36*, L13304, doi:10.1029/2009GL037235.

Thatcher, W. (1983), Nonlinear strain buildup and the earthquake cycle on the San Andreas fault, *J. Geophys. Res.*, *88*, 5893–5902, doi:10.1029/JB088iB07p05893.

Townend, J. (2006), What do faults feel? Observational constraints on the stresses acting on seismogenic faults, in *Earthquakes: Radiated Energy and the Physics of Faulting*, *Geophys. Monogr. Ser.*, vol. 170, edited by R. Abercrombie et al., pp. 313–327, AGU, Washington, D. C.

Vauchez, A., and A. Tomassi (2003), Wrench faults down to the asthenosphere: Geological and geophysical evidence and thermomechanical effects, *Geol. Soc. Spec. Publ.*, *210*, 15–34.

Watts, A. B. (1992), The effective elastic thickness of the lithosphere and the evolution of foreland basins, *Basin Res.*, *4*, 169–178, doi:10.1111/j.1365-2117.1992.tb00043.x.

Wdowinski, S., B. Smith-Konter, Y. Bock, and D. Sandwell (2007), Diffuse interseismic deformation across the Pacific–North America plate boundary, *Geology*, *35*, 311–314, doi:10.1130/G22938A.1.

West, D. P., and M. S. Hubbard (1997), Progressive localization of deformation during exhumation of a major strike-slip shear zone: Norumbega fault zone, south-central Maine, USA, *Tectonophysics*, *273*, 185–201, doi:10.1016/S0040-1951(96)00306-X.

Whitehouse, P. L., P. C. England, and G. A. Houseman (2005), A physical model for the motion of the Sierra Block relative to North America, *Earth Planet. Sci. Lett.*, *237*, 590–600, doi:10.1016/j.epsl.2005.03.028.

Wilson, C. K., C. H. Jones, P. Molnar, A. F. Sheehan, and O. S. Boyd (2004), Distributed deformation in the lower crust and upper mantle beneath a continental strike-slip fault zone: Marlborough fault system, South Island, New Zealand, *Geology*, *32*, 837–841, doi:10.1130/G20657.1.